Strojniški vestnik - Journal of Mechanical Engineering 70(2024)9-10, 426-439
DOI:10.5545/sv-jme.2023.884
Original Scientific Paper
Received for review: 2023-11-28
Received revised form: 2024-04-28
Accepted for publication: 2024-05-27

Simulation Research on the Control Method of Bow-Collapse in Gear Cold Roll-Beating

Qun Ma* – Li Cha – Xiangwei Zhang
Xi'an Technological University, School of Ordnance Science and Technology, China

Bow-collapse is a type of geometric defect in the gear cold roll-beating process. In order to effectively control bow-collapse and improve material utilization, this paper calculates the cross-section radius of the blank according to the volume invariance principle of metal plastic deformation, and then performs FE simulation of the cold roll-beating process by using the cyclic beating of adjacent tooth spaces and intermittent blank feeding method. The flow state of metal particles is investigated, revealing that the movement of metal particles along the axial direction of the blank is the main reason for the formation of bow-collapse. This paper proposes a method to correct the cross-section radius of the blank and thus control for bow-collapse, where the loss coefficient K characterizes the state of metal particle loss in an infinitesimal thickness region on the cross-section. The analytical equation for calculating the corrected value of the cross-section radius is derived, and the corrected value is calculated. Conducted on the modified blank, cold roll-beating FE simulation results show that bow-collapse is effectively controlled, and the loss coefficient K correctly reflects the loss state of metal particles on the cross-section. The simulation results also show that after cold roll-beating, the gear teeth with standard face width and tooth depth can be obtained after two turning end faces and turning tip circle processes. The bow-collapse control method proposed in this paper effectively improves material utilization.
Keywords: cold roll-beating, bow-collapse, FE simulation, loss coefficient, cross-section radius

Highlights

- *The reasons behind the formation of bow-collapse are revealed.*
- *A blank size modifying method is proposed to control the bow-collapse without limiting material flow.*
- *The loss coefficient K is defined to characterize the loss state of metal particles on the blank cross-section.*
- *The correction equation of the cross-section radius is derived, solved, and calculated.*
- *The effectiveness of the bow-collapse control method and the characterization of the metal particle loss state on the cross-section by the loss coefficient K are verified.*

0 INTRODUCTION

Cold roll-beating is a near-net forming process to produce gears via plastic deformation, and the advantages of this process include high productivity, short process chain, and high surface quality. The cold roll-beating forming motion consists of three parts: the rotation of the roller, the continuous indexing of the blank, and the feeding of the blank. The blank is a cylindrical bar, and the radius of its cross-section can be calculated according to the principle of volume invariance. However, after cold roll-beating, the blank produces geometric defects, such as flashes, concave tooth tips, and bow-collapses (Fig. 1).

Flashes can be removed by turning the end face. Concave tooth tips have little effect on the strength of the gear teeth and can be solved by removing materials other than the tip circle (e.g., the spline shaft in Fig. 2). Bow-collapse is a defect where the gear tooth appears high in the centre and low at both ends along the face width, similar to a bow shape (Fig. 1c). As the bow-collapse range is large and to ensure sufficient face width, the current solution is to increase the length of the blank, then all collapsed parts at both ends are removed after the gear is formed (Fig. 2). However, the above solution results in wasted material, and the material utilization rate is especially low when forming gear parts with small face width.

Fig. 1. *Geometric defects of cold roll-beating: a) concave tooth tips, b) flashes, and c) bow-collapse*

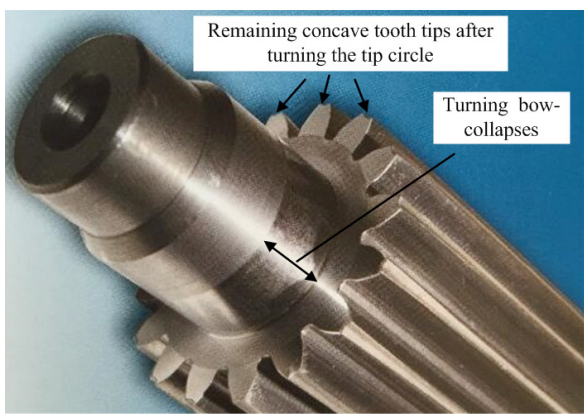

Fig. 2. *Spline shaft formed by the cold roll-beating process*

*Corr. Author's Address: Xi 'an Technological University, No. 2 Xuefu Middle Road, Xi'an, China, maqun@xatu.edu.cn

To control for geometric defects, such as bow-collapse, it is necessary to analyze the deformation process and material flow states to reveal the formation mechanism. While experimental studies are most consistent with real situations, measuring during the rolling process is challenging, and there is no clear physical evidence linking the results and parameters. In addition, it is difficult to show the plastic flow process of materials in experimental results. Current experimental studies on cold roll-beating are mainly on process parameters [1] and [2], surface forming characteristics [3], microstructure morphology [4] and [5], and residual stress analysis [6] and [7].

The development of finite element (FE) simulation technology has made it one of the most effective tools for studying complex metal plastic deformation processes and forming mechanisms. Byon et al. [8] predicted the crack growth length and growth direction in the steel strip rolling process via the FE method and verified the results with physical experiments. Nițu et al. [9] and [10] simulated a groove rolling process of complex profiles with the ABAQUS software and investigated the effects of radial force and blank diameter on productivity and groove quality. Hwang et al. [11] simulated the rolling process of aluminium wheels via the FE software and investigated the process parameters to improve geometric accuracy. Peng et al. [12] studied how material flow formed gear teeth during the cold rolling process via the FE method, then calculated tooth deviation and verified with experiments. Khodaee et al. [13] investigated the effects of blank geometry on tooth shape deviation via FE simulation and concluded that FE simulation can be used to optimize blank geometry in similar cold rolling cases. Li et al. [14] investigated the plastic deformation mechanism and material flow in the three rolling passes process of gears via FE analysis. Nistor et al. [15] investigated the influence of gear geometry, such as teeth number, and the deformation mechanism via FE analysis in terms of the evolution in tooth formation and formation loads. Ma and Zhang [16] calculated the cold roll-beating forming force via the FE simulation software DEFORM-3D, which was verified with experimental measurements. Deng et al. [17] conducted an FE simulation of the hot rolling process of face gear and verified the feasibility of hot rolling spur face gear. Li et al. [18] investigated the effects of initial bite depth, friction condition, and teeth number on the slippage in gear rolling via FE analysis and verified the result's reliability through experiments.

FE simulation is critical to understanding geometric defect control in the gear cold roll forming process. Wu et al. [19] proposed a gear-rolling process using conical gear rollers and used FE simulation to analyse the change of tooth shape and forming mechanism at different stages, where the bow-collapse and the rabbit ear defect (similar to the concave tooth tip in cold roll-beating) were in agreement with experimental results. Li et al. [20] simulated the gear rolling process through the FE software, and analysed the formation mechanism of rabbit ears, then verified the phenomenon and morphology of rabbit ears through experiments. Li et al. [21] investigated the formation causes and control methods of rabbit ear defects in gear roll forming via FE simulation. Ma et al. [22] investigated the optimization of rolling tools to reduce the height of rabbit ears during the roll-forming process through analytical models, FE methods, and experiments. Wu et al. [23] investigated the effect of the revised rollers on the control of rabbit ear defects through FE simulations and experiments, and the experimental results agreed with the simulation results. Ma et al. [24] investigated the effect of rolling parameters, the teeth number and rolling tools on rabbit ear defects. Current research on geometric defects mainly focuses on controlling rabbit ears, while there is no research on controlling bow-collapse.

Therefore, the paper uses FE simulation to study the control method of bow-collapse. First, the cross-section radius of the blank is calculated according to the volume invariance principle. Second, FE simulation of cold roll-beating is performed to analyse the deformation process and flow state of materials to reveal the causes for the formation of bow-collapse and to propose a method to control for bow-collapse. Last, the proposed bow-collapse control method is verified via FE simulation.

1 THEORETICAL CALCULATION OF THE CROSS-SECTION RADIUS OF THE BLANK

Fig. 3 illustrates the volume invariant principle to calculate the cross-section radius of the blank, where r_f and r_p are the root circle radius of the gear and the cross-section radius of the blank, respectively; A_1 and A_2 respectively represent the two diagonal shaded areas and A_3 is the area of the mesh. When the roller beats the blank, the metal in the tooth space is expected to produce plastic deformation, moving upward along the tooth flank to form a gear tooth, while metal on the other parts of the blank is not deformed. Therefore, the two diagonally shaded areas in Fig. 3 should be equal in area, which can be expressed as:

$$A_1=A_2=A-A_3, \tag{1}$$

where A is the area of a single tooth in the blank's cross-section.

The cross-section area of the blank is A_p, and $A_p=\pi r_p^2$. The area below the root circle of the gear is A_f, and $A_f=\pi r_f^2$. The area of all the teeth on the gear is Az, and z is the teeth number. According to the volume invariance principle, we get $A_p=A_f+Az$, and it can be expressed as:

$$\pi r_p^2=\pi r_f^2+Az.$$

Then, the cross-section radius of the blank can be determined with Eq. (2):

$$r_p=\sqrt{\frac{Az}{\pi}+r_f^2}. \tag{2}$$

For an involute spur gear, A can be expressed as [25] and [26]:

$$A=\frac{r_b^2}{3}\left(\tan^3\alpha_a-\tan^3\alpha_f\right)+r_a^2\left(\frac{\pi}{2z}+\text{inv}\alpha-\text{inv}\alpha_a\right)$$
$$-r_f^2\left(\frac{\pi}{2z}+\text{inv}\alpha-\text{inv}\alpha_f\right), \tag{3}$$

where r_b is the radius of the base circle, r_b is the radius of the tip circle, α, α_a and α_f are the pressure angles on the reference circle, the tip circle, and the root circle, respectively.

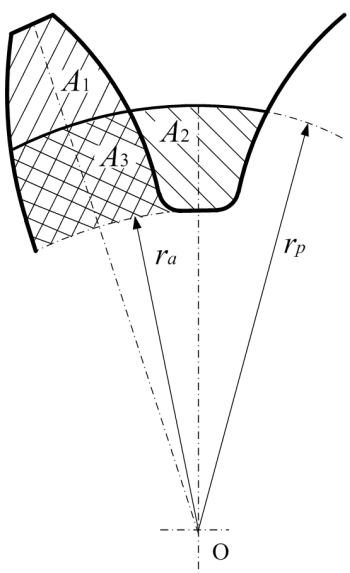

Fig. 3. *Volume invariant principle to calculate the cross-section radius of the blank*

For an involute spur gear with module $m=2$ and teeth number $z=20$, if $\alpha=20°$ and the modification coefficient is 0, it is known that $r_b=18.8$ mm, $r_f=17.5$ mm, $r_a=22$ mm and $\alpha_a=31.3°$. However, since $r_f<r_b$, the part below the base circle is no longer an involute but a fillet curve, so the area A of a single tooth cannot be calculated directly by Eq. (3).

The fillet curve below the base circle does not engage and is only related to the strength of the tooth root, so the fillet curve taken by different manufacturers is also different. The distance from the root circle to the base circle is only 1.3 mm, so an approximate calculation is made in this paper, as shown in Fig. 4. The fillet curve can be approximated as consisting of the straight line BC (B'C') and the circular arc CD (C'D'), where the straight line BC (B'C') is tangent to the involute line. Extending the straight lines BC and B'C', and intersecting with the root circle at the points E and E', then:

$$A=A_{ab}+A_{bf}+A_{cf}, \tag{4}$$

where A_{ab} is the area of the region between the tip circle and the base circle, A_{bf} is the area of the sector ring BB'E'E between the base circle and the root circle, and A_{cf} is the area of the region enclosed by the fillet curve, the root circle and the straight line CE (C'E').

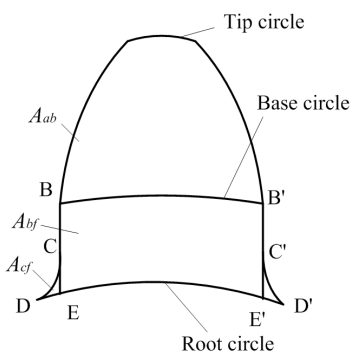

Fig. 4. *Calculation of tooth area A with an $m=2$ and $z=20$ involute spur gear*

Since the pressure angle on the base circle is 0, A_{ab} can be expressed as:

$$A_{ab}=\frac{r_b^2}{3}\tan^3\alpha_a+r_a^2\left(\frac{\pi}{2z}+\text{inv}\alpha-\text{inv}\alpha_a\right)$$
$$-r_b^2\left(\frac{\pi}{2z}+\text{inv}\alpha\right). \tag{5}$$

A_{bf} can be expressed as:

$$A_{bf}=\frac{\varphi_b}{2}\left(r_b^2-r_f^2\right), \tag{6}$$

where φ_b is the centre angle of the circle corresponding to points B and B'.

Then, φ_b can be expressed as:

$$\varphi_b = \frac{\pi}{z} + 2\text{inv}\alpha. \quad (7)$$

For A_{cf}, the arc DE can be approximated as a line segment perpendicular to the line CE, and both line segments DE and CE are tangent to the circular arc CD. If the radius of the circular arc CD is 0.5 mm, then $A_{cf} \approx 0.054$ mm^2.

With all parameters determined, the results are $A = 13.3$ mm^2 and $r_p = 19.8$ mm.

2 FE SIMULATION OF THE COLD ROLL-BEATING PROCESS

2.1 Establishment of the FE model

In order to observe the forming process of the gear tooth and analyse the causes of bow-collapse, the FE simulation software DEFORM-3D is used to simulate the cold roll-beating process. DEFORM-3D does not have a modelling function, so the 3D solid models are modelled with SOLIDWORKS.

2.1.1 Geometric Model of the Roller

The roller's geometric model of $m = 2$ and $z = 20$ involute spur gear is established. The profile curves of the roller coincide with the profile curves of the tooth space. The curves between the root circle and the base circle are the fillet curves shown in Fig. 4, and the curves above the base circle are two involutes. The maximum outside diameter of the roller is 40 mm and the thickness is 12.5 mm (Fig. 5).

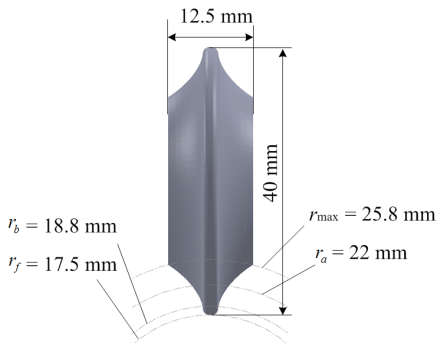

Fig. 5. *Geometric parameters of the roller*

2.1.2 Geometric Model of the Blank

The theoretical calculation of r_p is only a reference. Considering that the formation process of defects should be presented completely, so r_p cannot be a small value, and a slightly larger value will not affect the correction. Therefore, this paper increases r_p slightly and integers it to a value of $r_p = 20$ mm.

The FE simulation of metal plasticity requires significant computer resources and time, so it is meaningless to define the tooth width too large. If the definition of tooth width is very small and the distance between the front and back ends is very close, the movement law of metal particles along the axial direction of the blank cannot be fully presented. Therefore, the tooth width is set as 22 mm. Then the length of a part with a cross-section radius of 20 mm is set to 22 mm, and at the same time, there is a shaft with a diameter of 28 mm at each end face of the blank.

2.1.3 Importing Geometric Models

The geometric models of the roller and the blank are converted to STL data format and imported into the DEFORM-3D pre-processor (Fig. 6). Establishing a space rectangular coordinate system, the origin is located in the geometric centre of the blank, the Z-axis coincides with the axis of the blank, and the Y-axis is the symmetry axis of the profile curve of the tooth space formed by the roller.

The following definitions are established: The end face of the blank (Z = 11 mm) that is beat first is the front end face; the other end face (Z = –11 mm) is the back end face. The blank is divided into two parts along the XY plane: the part with Z $\geqslant$ 0 is the front half, and the part with Z < 0 is the back half.

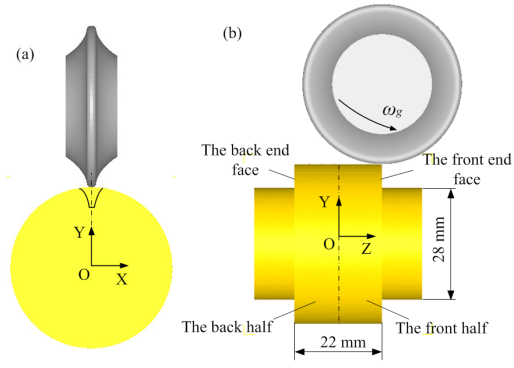

Fig. 6. *FE models in the DEFORM-3D pre-processor: a) the frontal view, and b) the left side view*

2.2 Pre-processing for Simulation

The simulation conditions in the DEFORM-3D pre-processor are set as follows:

(1) The motion parameters of cold roll-beating: The rotation speed of the roller is set as ω_g = 2000 r/min; the indexing angular speed of the blank is set as ω_p = 100 r/min; the feeding speed of the blank is set as v = 2 mm/r; and the rotation radius of the roller is set as R = 100 mm.
(2) Fully constrained boundary conditions are applied to the outer surfaces of the shafts with a diameter of 28 mm to simulate the clamping state of the blank in the cold roll-beating process.
(3) Disregarding the elastic deformation of the roller and the elastic restitution of the blank, the roller is defined as a rigid body, and the blank is defined as a plastic body. The material of the blank is set as Aluminium Alloy AL-1100.
(4) The blank is meshed, and the local mesh refinement is conducted in the main deformation zone to generate tetrahedral meshes. The element number is 217967, and min edge length is 0.1797 mm.
(5) Cutting fluid is used in the process of cold roll-beating, so it can be considered as pure rolling between the roller and the blank. To simplify the calculation, the friction coefficient between the roller and the blank is set to 0.
(6) Since cold roll-beating is conducted at room temperature, the simulation ambient temperature is defined to be constant at 20 °C.

2.3 FE Simulation of Cold Roll-Beating

Since the indexing and feeding speed of the blank is exceedingly low relative to the rotation speed of the roller, it has little effect on forming; the simulation of the beating process ignores the indexing and feeding movement of the blank, i.e., the blank is considered stationary.

In order to match the simulation process with the actual cold roll-beating process, two adjacent tooth spaces are cyclically beaten while the blank is intermittently fed. When the simulation of the 1st beating process of a tooth space is finished, the blank is rotated clockwise by 18° for the simulation of the 1st beating process of the adjacent tooth space. Then, the blank is rotated counterclockwise by 18° (back to the first tooth space), and at the same time, the blank is moved by 2 mm in the negative Z-axis direction to simulate the 2nd beating process of the first tooth space. Follow the above steps, alternately simulating the beating processes of two adjacent tooth spaces and moving the blank until both tooth spaces are fully formed.

The calculation results show that the longest action time of one beating process is less than 1.31×10^{-3} s, thus the time increment of the simulation is set as 1×10^{-5} s and the number of simulation steps is set as 140.

2.4 Simulation Results

Fig. 7 shows the FE simulation of the cold roll-beating process, and Fig. 8 shows the concave tooth tip, flashes, and bow-collapse formed by the FE simulation. As the blank is fed, the grooves gradually deepen, and the gear tooth gradually bulges, eventually forming a concave tooth tip, flashes, and bow-collapse similar to the shapes in Fig. 1.

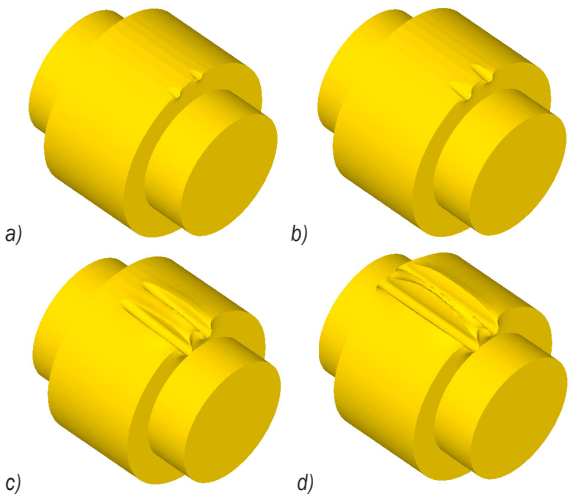

Fig. 7. *FE simulation of the cold roll-beating process: a) the 1st beating process of two tooth spaces, b) the 2nd beating process of two tooth spaces, c) the 11th beating process of two tooth spaces, and d) the final forming of two tooth spaces*

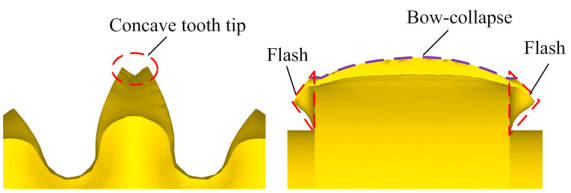

Fig. 8. *Geometric defects formed by FE simulation: the concave tooth tip and flashes and the bow-collapse*

2.5 Velocity Vector Diagrams of Metal Particles

The velocity vector diagrams of the metal particles when the roller moves to different positions are shown in Fig. 9:

(1) The flow state of metal particles in the front and back half of the blank is approximately the same. Metal particles mainly present two

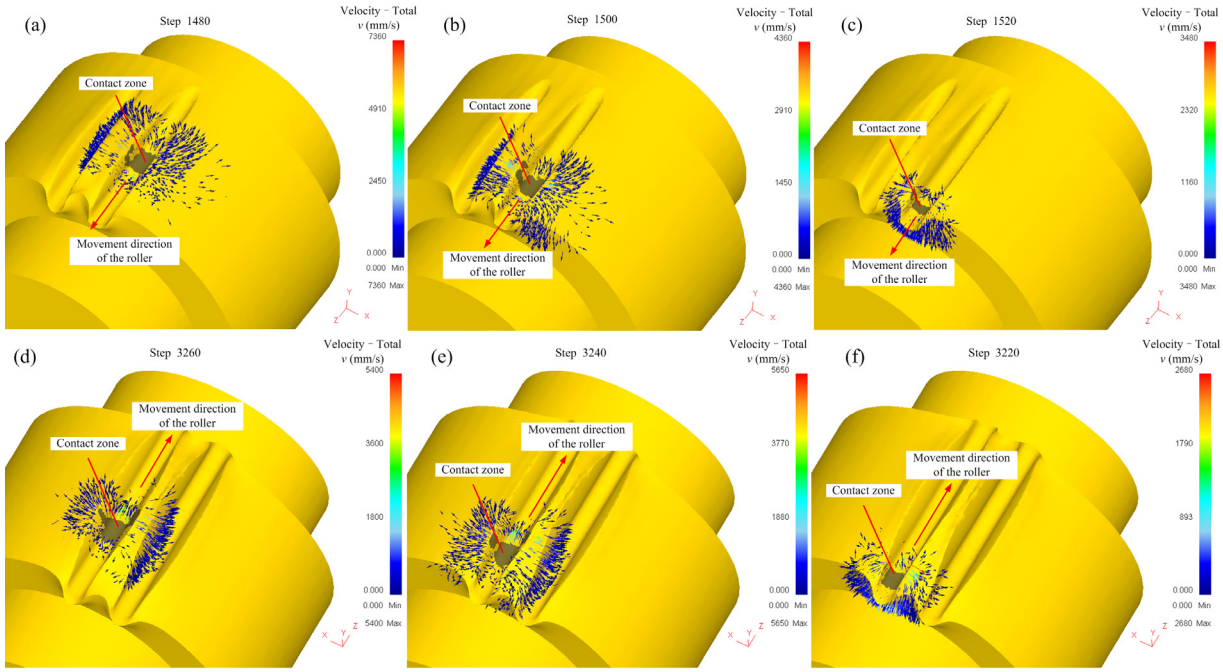

Fig. 9. *Velocity vectors of metal particles when the roller moves to different positions: a) the front half Z ≈ 5 mm, b) the front half Z ≈ 8 mm, c) the front half Z ≈ 11 mm, d) the back half Z ≈ –5 mm, e) the back half Z ≈ –8 mm, and f) the back half Z ≈ –11 mm*

motion states: one moving in the XY plane and the other moving perpendicular to the XY plane, i.e., moving along the Z-axis in the positive or negative directions.

(2) On the sides of the tooth space, metal particles are more likely to move in the XY plane, while on the bottom of the tooth space, metal particles are more likely to move perpendicular to the XY plane.

(3) Metal particles located in front of the roller move in the same direction as the roller, and metal particles located behind the roller move in the opposite direction to the roller, which is similar to the plastic deformation issue of a rigid cylinder rolling a rough surface **[27]** and **[28]**.

(4) The closer to the front and back end faces, the more obvious the movement trend of metal particles along the Z-axis. At the front end face, movement is mainly in the positive direction along the Z-axis, i.e., consistent with the roller, while at the back end face, movement is mainly in the negative direction along the Z-axis, i.e., opposite to the roller.

(5) When the roller beats a tooth space, metal particles of the adjacent tooth space also move, which proves that the cold roll-beating simulation of only a single tooth space is not consistent with actual working conditions.

2.6 Trajectory Tracking of Metal Particles

Trajectory tracking of metal particles is conducted using the point tracking tool in the DEFORM-3D post-processor to study the movement state of materials. Plastic deformation of materials outside the root circle is the main reason for the formation of tooth spaces and gear teeth. To simplify the calculation and consider for symmetry, the region X ∈ [–3.5, 0], Y ∈ [17, 20], and Z ∈ [–11, 11] on the blank before beating is taken, and the metal particles within are subjected to point tracking.

2.6.1 Moving State of Metal Particles in the Back Half of the Blank

Trajectory tracking is first performed on metal particles in the back half of the blank (Z ∈ [-11, 0]). Along the Z-axis direction, sections are taken at intervals of 1 mm, and a 17×9 array of particles is taken on each section, then trajectory tracking is performed for these 153 particles. The metal lattices are considered untwisted. Thus, the spatial position relationship between metal particles is unchanged, which is proven by analysing the trajectories of

metal particles at each simulation step. Due to the large amount of data, only the metal particle positions in the last simulation step are given in this paper to compare with the initial positions (Fig. 10).

(1) Movement of particles in the Z-axis direction

Metal particles in contact with the side profiles of the roller all show negative movement directions along the Z-axis, i.e., towards the back end face, and the closer to the back end face, the greater the displacement.

Metal particles below the roller (at the bottom of the tooth space), on the other hand, show two states of motion. In the range $Z \in (-5, 0]$, they move in the positive direction of the Z-axis, but as they approach the back end face ($Z \in [-11, -5]$), they move towards the back end face with increasing displacement.

(2) Movement of particles in the Y-axis direction

As shown in Fig. 10, combined with the velocity vectors of particles in Fig. 9, when farther away from the back end face, metal particles show more movement along the positive direction of the Y-axis, and when close to the back end face, the displacement of metal particles along the positive direction of the Y-axis decreases, and they gradually change to move along the negative direction of the Y-axis. In the range $Z \in [-11, -8]$, all metal particles transform to move in the negative direction of the Y-axis.

Most metal particles near the root circle move in the negative direction of the Y-axis, and metal particles within the root circle ($Y < 17.5$ mm) are also forced to move downwards.

2.6.2 *Moving State of Metal Particles in the Front Half of the Blank*

Fig. 11 shows the state of movement of metal particles in the front half of the blank. Compared to Fig. 10, the section positions of the pickup particles are only slightly different near the front end face.

As shown in Fig. 11, combined with the velocity vectors of particles in Fig. 9, the moving state of metal particles at the front half of the blank is essentially the same as that at the back half. Farther away from the front end face, metal particles mainly move along the positive direction of the Y-axis, while the closer to the front end face, the greater the displacement of metal particles along the negative direction of the Y-axis and the positive direction of the Z-axis.

2.7 Analysis and Discussion

(1) As shown in Figs. 10 and 11, the closer to the front (back) end face, the greater the displacement

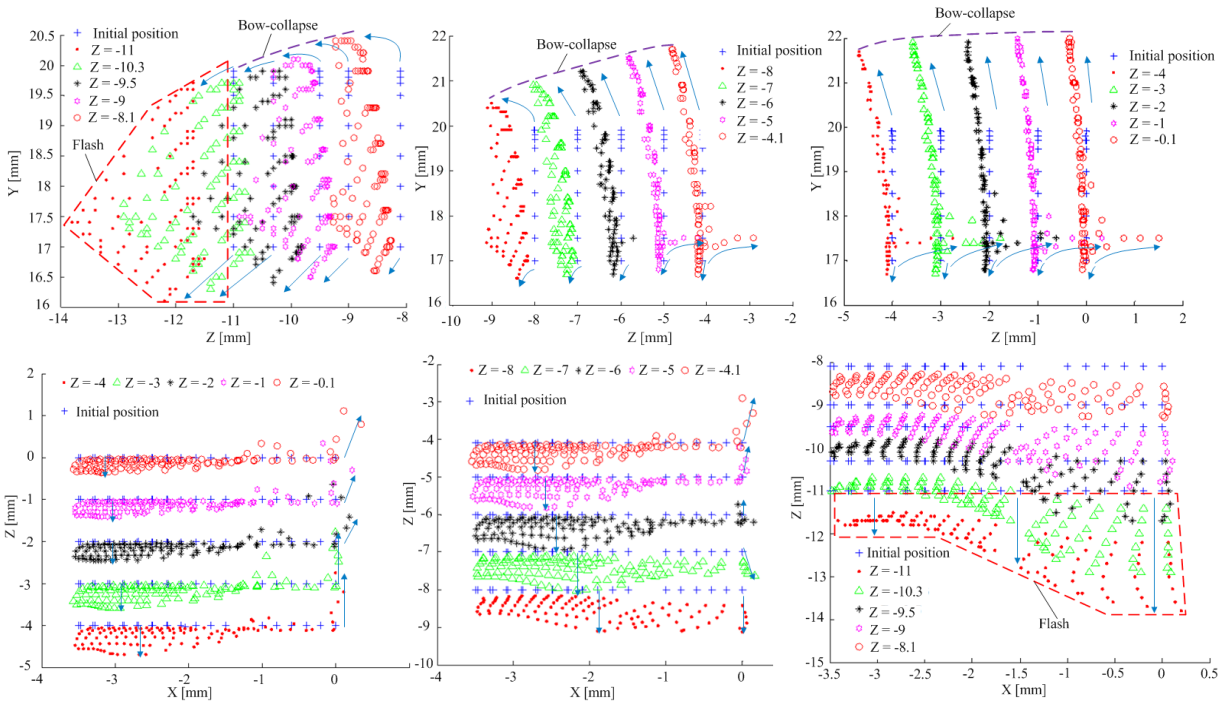

Fig. 10. *Movement of metal particles in the back half of the blank*

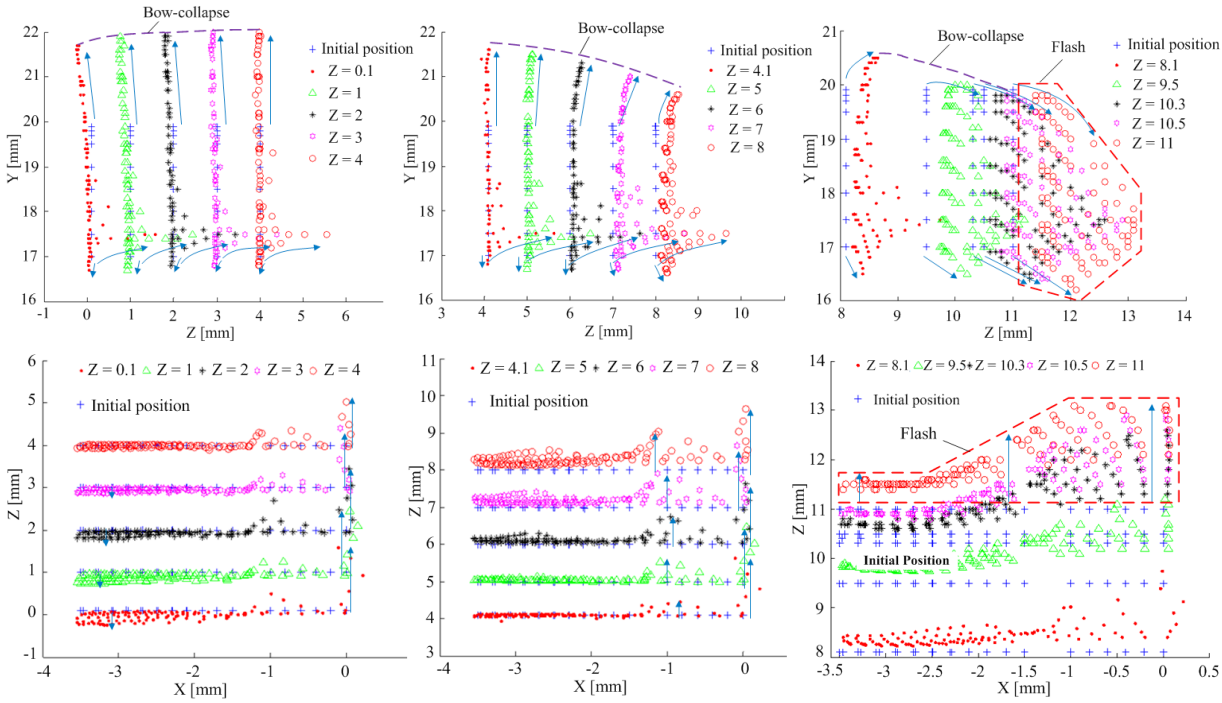

Fig. 11. *Movement of metal particles in the front half of the blank*

of metal particles along the positive (negative) direction of the Z-axis, and a large number of metal particles near the front (back) end face move out of the range of the face width, forming flashes. The reason for this phenomenon is that the end faces and the outer surface of the blank are all free surfaces; according to the principle of least resistance to plastic flow of metals, the closer to the end faces, the resistance of metal particles to move along the Z-axis direction is smaller. Thus, they move towards the end faces. Away from the end faces, most metal particles have less resistance to move towards the outer surface of the blank, and they show more upward movement along the tooth flank, forming a raised gear tooth.

(2) The movement along the XY plane does not cause the loss of metal particles on the cross-section of the blank, whereas the movement along the Z-axis direction leads to the loss of metal particles on the cross-section, which is the main cause for the formation of bow-collapse.

(3) Bow-collapse can only be controlled in two ways, either by limiting the movement of metal particles along the Z-axis or by increasing the cross-section radius of the blank to replace the lost metal particles.

3 CORRECTION OF THE CROSS-SECTION RADIUS OF THE BLANK

As mentioned above, limiting the movement of metal particles along the Z-axis direction is a method to control bow-collapse, which can be achieved with two approaches. The first is to limit the front and back end faces, which can be realized by clamping the front and back end faces with special fixtures, but the fixtures will affect the movement of the roller, thus failing to form a complete tooth space. The second is to increase the axial length of the blank so that metal particles within the face width move away from the front and back end faces, then turning to remove the collapsed part, which is consistent with the current production process, as shown in Fig. 2. The second approach results in a waste of materials and also complicates the machining process.

Therefore, this paper proposes a method to control the metal plastic forming geometry, which does not limit the plastic flow of the material but modifies the blank size to supplement (or reduce) the lack (or excess) of material in the forming process. For the bow-collapse of cold roll-beating, it is necessary to increase the cross-section radius of the blank.

As shown in Fig. 3, according to the volume invariance principle, $A_1=A_2=A-A_3$. However, due to the movement of metal particles along the Z-axis,

A_1 changes to A_1' and A_2 remains unchanged so that $A_1' \leq A_2$.

In this paper, we define the loss coefficient K as:

$$K = \frac{A_2 - A_1'}{A_2}. \tag{8}$$

It is assumed that the loss coefficient K is independent of the size of the cross-section and is only related to the axial position. In this paper, the loss coefficient K is used to characterize the proportion of metal particles lost in an infinitesimal thickness region on the cross-section. Since $A_1' \leq A_2$, in general $0 \leq K \leq 1$.

By increasing the cross-section radius r_p, A_2 and d, A_3 also increase, but the loss coefficient K is unchanged. Assuming that A_2 and A_3 become A_2' and A_3', cross-section radius r_p is the corrected value when Eq. (9) is satisfied.

$$A_1' = (1-K)A_2' = A - A_3. \tag{9}$$

Therefore, the correction method for the cross-section radius r_p is:

(1) Calculate A_1' and A_2 based on the results of the FE simulation,
(2) Calculate the loss coefficient K via Eq. (8);
(3) Calculate A_2' on the blank's cross-section;
(4) Increasing the cross-section radius r_p until Eq. (9) is satisfied.

3.1 Calculation of A_1' and A_2

The concave tooth tip should be included in the calculations of A_1'. Fig. 12 shows the shape of the concave tooth tip in the Z = 0 cross-section. The forces on both sides of the gear tooth are essentially identical, and, as can be seen from Figs. 1 and 12, the concave tooth tips are approximately symmetrically distributed along the centre of the gear tooth. However, as shown in Fig. 7d, the shapes and sizes of the concave tooth tip varies across different cross-sections, so it is difficult to accurately calculate the area of concave tooth tips.

Here, we calculate the average depth of the gear tooth containing concave tooth tips and then calculate A_1' according to the tooth area calculations.

Therefore, the average gear tooth depth H can be estimated via Eq. (10), which is expressed as:

$$H \approx \frac{H_{\max} + H_{\min}}{2}, \tag{10}$$

where $H_{\max}$ is the distance from the highest point of the concave tooth tip to the root circle; $H_{\min}$ is the distance from the lowest point of the concave tooth tip to the root circle.

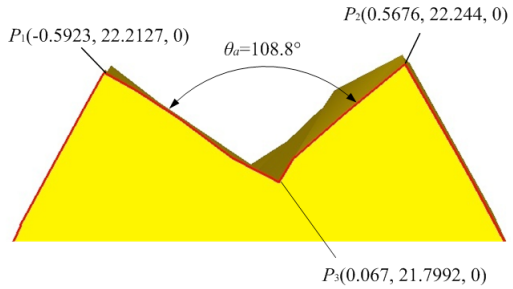

Fig. 12. *The concave tooth tip on the cross-section Z=0 (in mm)*

In the DEFORM-3D post-processor, the coordinates of the highest and lowest points of the concave tooth tip are extracted at 0.5 mm intervals along the Z-axis direction. The average gear tooth depth H is calculated via Eq. (10) and fitted to a smooth curve (Fig. 13). The minimum value of H appears at the two end faces, even lower than the outer surface of the blank, and only in the range of Z ∈ [-2, 0.5] which basically reaches the standard full tooth depth (4.5 mm).

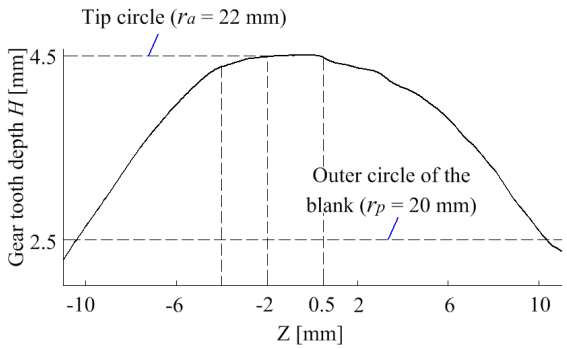

Fig. 13. *Variations of the average gear tooth depth*

Assuming that the radius of the tip circle after cold roll-beating is r_i, since the gear tooth depth is insufficient, we have $r_i < r_a$.

At this point, A_1' can be calculated via Eq. (11) and expressed as:

$$A_1' = \frac{r_b^2}{3}\left(\tan^3\alpha_i - \tan^3\alpha_p\right) + r_i^2\left(\frac{\pi}{2z} + \text{inv}\alpha - \text{inv}\alpha_i\right) - r_p^2\left(\frac{\pi}{2z} + \text{inv}\alpha - \text{inv}\alpha_p\right), \tag{11}$$

where a_i is the pressure angle at the tip circle, and α_p is the pressure angle at the outer circle of the blank.

$\alpha_p = \arccos(r_b/r_p)$, $\alpha_i = \arccos(r_b/r_i)$, and r_i can be determined by the gear tooth depth curve in Fig. 13.

Since A_2 does not change, it can still be expressed as $A_2=A-A_3=A_1$, then A_2 can be calculated via Eq. (12):

$$A_2=\frac{r_b^2}{3}\left(\tan^3\alpha_a-\tan^3\alpha_p\right)+r_a^2\left(\frac{\pi}{2z}+\text{inv}\alpha-\text{inv}\alpha_a\right)-r_p^2\left(\frac{\pi}{2z}+\text{inv}\alpha-\text{inv}\alpha_p\right), \quad (12)$$

3.2 Calculation of the Loss Coefficient K

From the results of A_1' and A_2, the loss coefficient K is calculated for any cross-section of the blank and fitted to a smooth curve (Fig. 14).

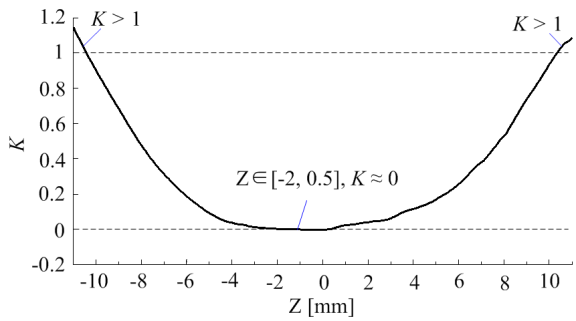

Fig. 14. *Variations of loss coefficient K*

It should be noted that the loss coefficient $K>1$ when close to the front and back end faces. In comparison with Fig. 13, near the front and back end faces, the radius of the tip circle formed by cold roll-beating is smaller than the cross-section radius of the blank, thus A_1' is negative, which shows that $K>1$. Once a flash is created, the lower surface of the flash is also a free surface so that near the front and back faces, the metal particles move not only along the Z-axis but also downwards. This results in the formation of collapse instead of raised gear teeth near the front and back end faces.

3.3 Correction Equation for the Cross-Section Radius r_p

The calculation of A_2' on the cross-section of the blank is given in Fig. 15. Increasing r_p so that the gear tooth depth reaches the standard value, the corrected A_2 becomes A_2', and therefore A_2' cannot be calculated via Eq. (12).

Make the outer circle of the blank intersect the tooth profile curves of two adjacent gear teeth at points N and P. Make the root circle intersect the straight lines NO and PO at points N' and P'.

Since the areas of the two mesh regions in Fig. 15 are equal, i.e., $A_{r1}=A_{r2}$, the corrected A_2' can be expressed as:

$$A_2'=A_{NN'P'P}-A_3', \quad (13)$$

where $A_{NN'P'P}$ is the area of the sector ring $NN'P'P$ with an angular pitch of θ_P.

A_3' is the area of a single gear tooth within the blank outer circle after the increase of r_p. Although A_3' in Fig.15 increases due to the increase of r_p, it can still be expressed as:

$$A_3'=A-A_1'. \quad (13)$$

Substitute Eq. (14) into Eq. (13), and we get:

$$A_2'=A_{NN'P'P}-A+A_1'. \quad (14)$$

Since K is independent of the cross-section size and is only related to the cross-section position, $A_1'=(1-K)A_2'$ still holds, then the correction equation for the cross-section radius can be given as:

$$A_1'-(1-K)A_2'=A_1'-(1-K)(A_{NN'P'P}-A+A_1')=0. \quad (15)$$

After collating, we get:

$$KA_1'-(1-K)(A_{NN'P'P}-A+A_1')=0. \quad (16)$$

$A_{NN'P'P}$ can be calculated by Eq.(17):

$$ANN'P'P=\frac{\theta_p\left(r_p^2-r_f^2\right)}{2}, \quad (17)$$

where, $\theta_P=2\pi/z$.

As shown in Fig. 15, N and P are located on the left tooth surface of the adjacent gear teeth, respectively, and are also on the same circle with r_p as the radius. Therefore, whether the teeth number is odd or even, and regardless of the value of r_p, $\theta_P=2\pi/z$ is satisfied.

Increasing r_p so that $r_i=r_a$, we have:

$$A_1'=\frac{r_b^2}{3}\left(\tan^3\alpha_a-\tan^3\alpha_p\right)+r_a^2\left(\frac{\pi}{2z}+\text{inv}\alpha-\text{inv}\alpha_a\right)-r_p^2\left(\frac{\pi}{2z}+\text{inv}\alpha-\text{inv}\alpha_p\right). \quad (18)$$

Substitute Eq. (17) and Eq. (18) into Eq. (16):

$$K\left[\frac{r_b^2}{3}\left(\tan^3\alpha_a-\tan^3\alpha_p\right)+r_a^2\left(\frac{\pi}{2z}+\text{inv}\alpha-\text{inv}\alpha_a\right)-r_p^2\left(\frac{\pi}{2z}+\text{inv}\alpha-\text{inv}\alpha_p\right)\right]-(1-K)\left[\frac{\pi\left(r_p^2-r_f^2\right)}{z}-A\right]=0. \quad (19)$$

Since α_P can be written as a function of r_p, i.e., $\alpha_P=\arccos(r_b/r_p)$, Eq. (19) is the correction equation for the cross-section radius with r_p as the variable.

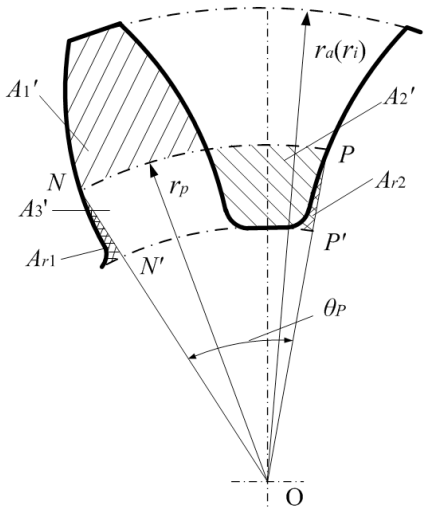

Fig. 15. *Method of calculating A_2'*

3.4 Correction of the Cross-Section Radius r_p

It is difficult to directly solve the transcendental equation given by Eq. (19). Therefore, in this paper, we use MATLAB to prepare a program to iteratively calculate the approximate numerical solution of r_p. Considering that the corrected value of r_p should be larger than the theoretically calculated cross-section radius and smaller than the radius of the tip circle, the solution interval for r_p is set to [19.8, 22]. The solution is fitted to a smooth curve (Fig. 16).

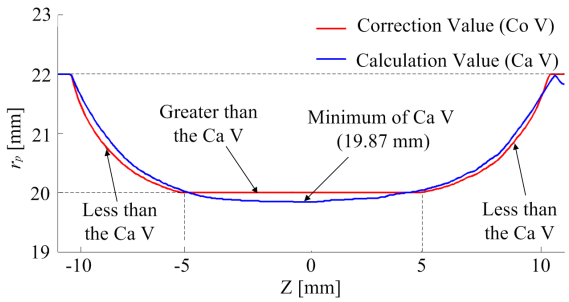

Fig. 16. *Values of r_p in calculation and in correction*

By analysing the variations of r_p, we get:

(1) r_p varies little in the range of $Z \in [-5, 5]$, with a minimum value of 19.87 mm and a maximum value of roughly 20 mm.

(2) The variation curve of r_p is roughly symmetrically distributed with respect to the Z=0 cross-section.

(3) r_p transitions from Z=±11 along an approximate circular curve to Z=±5.

Based on the variation curve of r_p, and also considering that the blank is easy to machine, r_p is corrected as follows:

(1) Taken according to a symmetric distribution with respect to the Z=0 cross-section.

(2) Taken as a constant value in the range of $Z \in [-5, 5]$.

(3) Taken as a circular curve in the interval from Z=±10 to Z=±5 to facilitate the machining of the blank.

(4) After the gear is formed, the edges of two end faces are generally chamfered, so the corrected values of r_p in the ranges of $Z \in [-11, -10]$ and $Z \in [10, 11]$ are taken as the values at Z = ±10.

According to the above principles, the corrected values of r_p at Z=±10 and Z=±5 are set as 22 mm and 20 mm, respectively (Fig. 16).

3.5 FE Simulation of Cold Roll-Beating of the Corrected Blank

The 3D models of the corrected blank and the roller are imported into the DEFOEM-3D pre-processor, and chamfers of 1×45° are added to the edges of end faces (Fig. 17a). The simulation is still conducted in accordance with the method of the cyclic beating of adjacent tooth spaces and intermittent feeding of the blank; the simulation results are shown in Fig. 17b.

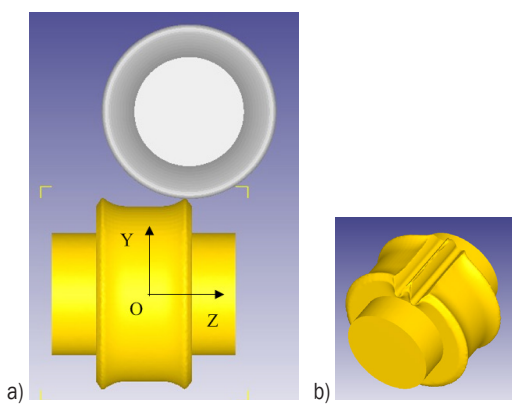

Fig. 17. *FE simulation of cold roll-beating of the corrected blank: a) the pre-processing models, and b) the simulated gear tooth*

Fig. 18 shows the top profile curve of the gear tooth. The middle of the curve is slightly higher, and there are small collapses on both sides, which indicate that the bow-collapse is effectively controlled. Compared with Fig. 16, the top profile curve of the gear tooth in Fig. 18 is in good agreement with the differences between the correction and calculation values given in Fig. 16.

Comparing Fig. 18 with Fig. 8b, flashes of the corrected blank are obviously larger. According to the definition of the loss coefficient K in this paper, the loss of metal particles on the cross-section can be expressed as KA_2. Near the end faces, there is $A_2' > A_2$, while K is unchanged, so the loss of metal particles near the end faces after correction (expressed as KA_2') is larger than that of the blank before correction (expressed as KA_2), i.e., the flashes of the blank after correction are larger than those of the blank before correction.

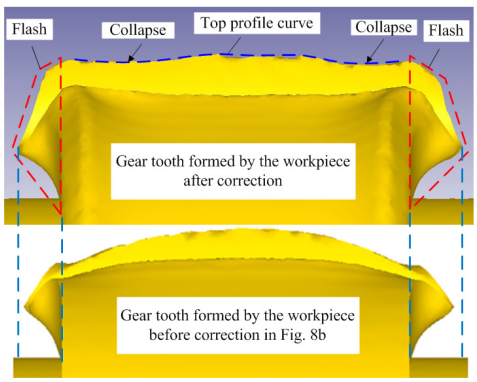

Fig. 18. *Top profile curve of the gear tooth and the flash compared with Fig. 8b*

In the DEFORM-3D post-processor, the part above 22 mm is removed using the Slicing tool with a plane (Y = 22) tangent to the top land of the gear tooth (Fig. 19). It can be seen that the rest of the part reaches the top land, except for a small pit on each of the position corresponding to the two collapses in Fig. 18. The maximum height of the cut-off part is only 1.05 mm, which indicates that the correction of r_p has controlled for bow-collapse, and also proves that the loss coefficient K correctly reflects the state of loss of metal particles on the cross-section.

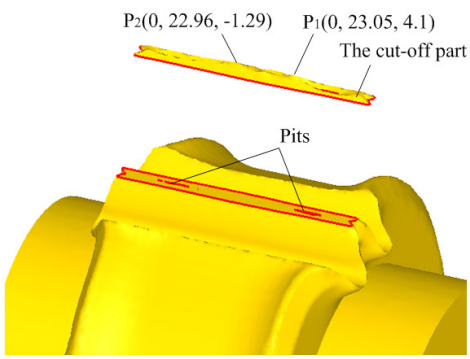

Fig. 19. *Slicing of the top land of the gear tooth (in mm)*

Using the slicing tool, the parts other than the gear tooth are removed, and a gear tooth with standard face width and tooth depth is obtained (Fig. 20).

Fig. 20 shows that after cold roll-beating, the flashes and concave tooth tips can be removed by two processes: turning the tip circle and turning end faces, resulting in a standard tooth depth and full face width. This bow-collapse control method removes relatively less material and improves material utilization.

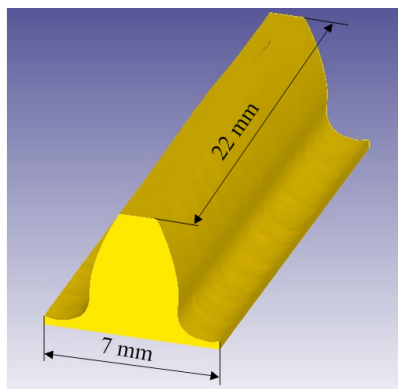

Fig. 20. *Gear tooth with standard tooth depth and full face width*

4 CONCLUSIONS

(1) According to the volume invariant principle of metal plastic deformation, the cross-section radius of the blank is calculated, the FE simulation of the cold roll-beating process is conducted with the cyclic beating of adjacent tooth spaces and intermittent blank feeding method, and geometric defects are obtained in accordance with the actual situation.

(2) Metal particles roughly present two motion states: movement perpendicular to the blank axis (in the XY plane) and movement along the blank axis (in the Z-axis direction), and the latter is the main reason for the formation of bow-collapse.

(3) The corrected value of the cross-section radius is calculated by solving the analytical equation with the iterative method, and the corrected blank is subjected to cold roll-beating FE simulation. The results show that bow-collapse is controlled, and the loss coefficient K correctly reflects the state of loss of metal particles on the cross-section.

(4) The simulation results prove that after cold roll-beating of corrected blank, gear teeth with standard face width and tooth depth can be obtained by turning the tip circle and turning end faces. Bow-collapse can be controlled, and material utilization can be improved by the

method proposed in this paper for correcting the cross-section radius of the blank.

5 SCIENTIFIC AND INDUSTRIAL CONTRIBUTIONS

(1) The loss coefficient K is introduced to characterize the loss state of metal particles on the cross-section of the blank, and the analytical equation for calculating the correction value of the cross-section radius of the blank is derived. This work provides a calculation method for determining the size correction of blank in metal plastic forming.
(2) The correction method studied in this paper can be applied to cold roll-beating production of spline, optimize the cold roll-beating process, shorten the process chain, and improve material utilization rate.

6 PROSPECTS FOR FUTURE RESEARCH

(1) Conducting experimental studies on the control method of bow-collapse is a direction for future research. Modifications of ordinary machine tools to meet the requirements of cold roll-beating forming motion have been reported in experimental studies of cold roll-beating process parameters and force-energy parameters **[1]** to **[3]**, and **[16]**. However, for the study of geometry control, equipment is required to have higher structural stability and sufficient power, which is difficult to accomplish with ordinary machine tools. The design of specialized cold roll-beating experimental equipment is a prerequisite for the experimental study of geometry control.
(2) As mentioned above, of the two methods of controlling bow-collapse, the method investigated in this paper is the second method, which does not control the flow of materials, but supplements the loss caused by the flow of the materials. The first method, controlling the flow of materials, although not easy to achieve, is the essence of plastic forming of metal and the method with the highest material utilization. Controlling the flow of materials by reasonably designing fixtures of the blank and the shape of the roller and ensuring the cold roll-beating forming movement is also a direction for future research.

7 REFERENCES

[1] Li, L., Li, Y., Yang, M., Xiao, X., Cui, L., Cui, F. (2019). Effects of process parameters on forming force and accuracy in cold roll-beating forming external tooth groove. *The International Journal of Advanced Manufacturing Technology*, vol.100, p. 2229-2242, **DOI:10.1007/s00170-018-2844-6**.

[2] Li, L., Li, Y., Yang, M., Tong, T. (2019). Process parameters decision to optimization of cold rolling-beating forming process through experiment and modeling. *Metals*, vol. 9, no. 4, 405, **DOI:10.3390/met9040405**.

[3] Yang, M., Li, Y., Duan, H., Li, Y. (2015). Scale-like texture defect of slab metal cold roll-beating. *Materials Research Innovations*, vol. 19, p. 911-915, **DOI:10.1179/1432891714Z.0000000001220**.

[4] Niu, T., Li, Y., Liu, Z., Qi, H. (2018). Forming mechanism of high-speed cold roll beating of spline tooth. *Advances in Materials Science and Engineering*, vol. 2018, **DOI:10.1155/2018/2892361**.

[5] Cui, F., Su, Y., Wang, X., Yu, X., Ruan, X., Liu, L. (2018). Surface work-hardening optimization of cold roll-beating splines based on an improved double-response surface-satisfaction function method. *Advances in Mechanical Engineering*, vol. 10, no. 6, **DOI:10.1177/1687814018782630**.

[6] Cui, F., Su, Y., Xie, K., Wang, X., Ruan, X., Liu, F. (2018). Analysis of metal flow behavior and residual stress formation of complex functional profiles under high-speed cold roll-beating. *Advances in Materials Science and Engineering*, vol. 2018, no. 1, 9672768, **DOI:10.1155/2018/9672768**.

[7] Ding, Z.H., Cui, F.K., Liu, Y., Li, Y., Xie, K (2017). A model of surface residual stress distribution of cold rolling spline. *Mathematical Problems in Engineering*, vol. 2017, no. 1, 2425645, **DOI:10.1155/2017/2425645**.

[8] Byon, S.M., Roh, Y., Yang, Z., Lee, Y. (2020) A roll-bending approach to suppress the edge cracking of silicon steel in the cold rolling process. *Proceedings of the Institution of Mechanical Engineers, Part B: Journal of Engineering Manufacture*, vol. 235, no. 1-2, p. 112-124, **DOI:10.1177/0954405420949221**.

[9] Nițu, E., Iordache, M., Marincei, L., Charpentier, I., Le Coz, G., & Ferron, G., Ungureanu, I. (2011). FE-Modeling of Cold Rolling by In-Feed Method of Circular Grooves. *Strojniški vestnik - Journal of Mechanical Engineering*, vol. 57, no. 9, p. 667-673, **DOI:10.5545/sv-jme.2010.244**.

[10] Nitu, E.L., Iordache, D.M., Badulescu, C. (2021). Numerical investigation of the radial cold rolling process of the grooves. *Proceedings of the Institution of Mechanical Engineers, Part B: Journal of Engineering Manufacture*, vol. 236, no. 3, p. 233-244, **DOI:10.1177/09544054211024571**.

[11] Hwang, S.Y., Kim, N., Lee, C. (2015). Numerical investigation on the effect of process parameters during aluminum wheel flow-forming. *Strojniški vestnik - Journal of Mechanical Engineering*, vol. 61, no. 7-8, p. 471-476, **DOI:10.5545/sv-jme.2014.2180**.

[12] Peng, B., Luo, Y., Wang, H., Niu, T., Wang, Y. (2023). Investigation on the effects of tooth profile deviation in gear rolling process. *The International Journal of Advanced Manufacturing Technology*, vol. 126, no. 5, p. 1877-1887, **DOI:10.1007/s00170-023-11207-5**.

[13] Khodaee, A., Melander, A., Haglun, S. (2018). The effects of blank geometry on gear rolling for large gear modules:

Experiments and finite element simulations. *IEEE Access*, vol. 6, p. 33344-33352, **DOI:10.1109/ACCESS.2018.2847737**.

[14] Li, K., Zhang, D., Zhao, S., Zhang, P., Fei, L. (2023). A novel multipass incremental gear rolling process with blank and rolling die axes crossed. *The International Journal of Advanced Manufacturing Technology*, vol. 129, no. 1, p. 715-726, **DOI:10.1007/s00170-023-12314-z**.

[15] Nistor, L., Neag, A., Marian, I., Frunza, D. (2016). Experimental and numerical simulation study of simultaneous toothing of spur gears by press-rolling process. *Journal of Manufacturing Science and Engineering*, vol.138, no. 12, **DOI:10.1115/1.4034493**.

[16] Ma, Q., Zhang, X. (2023). Research on an analytical method for the forming force of external spline cold roll-beating. *Strojniški vestnik - Journal of Mechanical Engineering*, vol. 69, no. 9-10, p. 409-421, **DOI:10.5545/sv-jme.2023.616**.

[17] Deng, J., Jiang, C., Deng, X., Fu, Y., Wang, Z. (2023). Numerical simulation and experimental study on hot rolling forming of spur face gears. *Advances in Mechanical Engineering*, vol. 15, no.9, p. 1679603520, **DOI:10.1177/16878132231190336**.

[18] Li, J., Wang, G., Wu, T. (2016). Numerical simulation and experimental study of slippage in gear rolling. *Journal of Materials Processing Technology*, vol. 234, p. 280-289, **DOI:10.1016/j.jmatprotec.2016.03.030**.

[19] Wu, T., Wang, G., Li, J., Yan, K. (2018). Investigation on gear rolling process using conical gear rollers and design method of the conical gear roller. *Journal of Materials Processing Technology*, vol. 259, p. 141-149, **DOI:10.1016/j.jmatprotec.2018.04.034**.

[20] Li, D., Zhang, S., Yang, X., Ma, H., Sun, S. (2020). Numerical investigation on roll forming of strai-ght bevel gear. *The International Journal of Advanced Manufacturing Technology*, vol. 107, no. 3, p. 1517-1537, **DOI:10.1007/s00170-020-05004-7**.

[21] Li, J., Wang, G., Wu, T. (2017). Numerical-experimental investigation on the rabbit ear formation mechanism in gear rolling. *The International Journal of Advanced Manufacturing Technology*, vol. 91, no. 9, p. 3551-3559, **DOI:10.1007/s00170-017-0009-7**.

[22] Ma, Z., Luo, Y., Wang, Y., Mao, J. (2018). Geometric design of the rolling tool for gear roll-forming process with axial-infeed. *Journal of Materials Processing Technology*, vol. 258, p. 67-79, **DOI:10.1016/j.jmatprotec.2018.03.006**.

[23] Wu, T., Wang, G., Li, J., Yan, K. (2019). Structure design and effects of conical gear roller on restraining rabbit ear defects during gear rolling. *The International Journal of Advanced Manufacturing Technology*, vol. 103, p. 1621-1631, **DOI:10.1007/s00170-019-03730-1**.

[24] Ma, Z., Tian, Y., Zhang, F., Liu, J., Luo, Y. (2023). Theoretical and experimental study on influencing factors of rabbit ear in the gear forced through feed rolling process. *The International Journal of Advanced Manufacturing Technology*, vol. 127, p. 4641-4658, **DOI:10.1007/s00170-023-11787-2**.

[25] Peng, S., Peng, S. (2011). Algorithms research on tooth profile volume of involute profile cylindrical part. *Die and Mould Technology*, vol. 6, p. 1-4 (in Chinese).

[26] Peng, S., Wu, X., Peng, S. (2012). Application research on involute profile area algorithm in cold rolling technology. *Die and Mould Technology*, vol. 1, p. 8-11 (in Chinese).

[27] Nepershin, R.I. (2013). Plastic deformation of surface layer during rigid cylinder rolling and sliding. *Journal of Friction and Wear*, vol. 34, p. 204-207, **DOI:10.3103/S1068366613030112**.

[28] Nepershin, R.I. (2019). Plastic deformation of a rough surface by the rigid rolling cylinder. *Journal of Friction and Wear*, vol. 40, p. 65-72, **DOI:10.3103/S1068366619010148**.